Nuclear Materials and Energy 34 (2023) 101356

Contents lists available at ScienceDirect

Nuclear Materials and Energy

journal homepage: www.elsevier.com/locate/nme

Modeling deep slot divertor concepts at DIII-D using SOLPS-ITER with drifts

R. Maurizio [a,b,*], A.W. Leonard [b], A.G. McLean [c], M.W. Shafer [d], P.C. Stangeby [e], D. Thomas [b], J.H. Yu [b]

[a] Oak Ridge Associated Universities, Oak Ridge, 37830 TN, USA
[b] General Atomics, San Diego, 92186 CA, USA
[c] Lawrence Livermore National Laboratory, Livermore, 94550 CA, USA
[d] Oak Ridge National Laboratory, Oak Ridge, 37831 TN, USA
[e] University of Toronto, Toronto, ON, M3H 5T6, Canada

ARTICLE INFO

Keywords:
SOLPS-ITER
DIII-D
Divertor
Detachment
Slot divertor

ABSTRACT

A staged divertor program is currently under discussion to advance DIII-D research on core-edge integration. One phase could address optimization of power and particle exhaust, and supporting modeling of several slot divertor options is underway, including variations in wall baffling, slot depth and divertor leg length. This paper focuses on the role of slot depth to achieve highly dissipative (detached) divertor conditions, in both B_T directions. For ion $\mathbf{B}\times\nabla B$ into the divertor and P_{SOL} = 4 MW, SOLPS-ITER finds that increasing the slot depth from 18 to 50 cm reduces the upstream separatrix electron density needed to detach by 15%, due to increased divertor radiation. A dedicated run of the EIRENE neutral transport code, in which neutrals are launched from the outer target and followed until ionization, finds that neutral leakage is strongly reduced in the deep slot compared to the shallow slot, explaining the increased divertor radiation and, thus, lower detachment density threshold. Reversing the B_T direction cools and densifies the plasma in the slot, such that both slot options are detached at all simulated densities. As for the opposite B_T direction, the deep slot has lower target temperature compared to the shallow slot, as a result of lower neutral leakage. Increasing the depth of a slot divertor is, therefore, beneficial to achieve highly dissipative divertor conditions for both field directions. Additional modeling will build on these results to evaluate whether an increased slot depth can also improve trapping of low-Z radiating impurities.

1. Introduction

A staged divertor program is currently under discussion to advance DIII-D research on core-edge integration toward the qualification of scenarios for future Fusion Pilot Plant designs. Initially, the idea in DIII-D would be for the poloidal extent of a new upper divertor to remain short to maximize the plasma volume for Advanced Tokamak scenarios. Then, a second phase of the program could replace the upper divertor structure with a more intrusive larger volume divertor for optimization of power and particle exhaust. A final phase could target combined core-divertor optimization.

For the second phase mission, extensive modeling activities are underway at DIII-D to investigate the power exhaust properties of several slot design options, using the SOLPS-ITER code package with particle drift effects, in high triangularity and low radius plasmas with the upper single-null configuration. The explored options include different degrees of wall baffling on both the private and common flux side, variations in the slot depth and in the outer divertor leg length.

In the framework of these modeling efforts, this paper specifically evaluates the role of slot depth to achieve highly dissipative (detached) divertor conditions, thus advancing the international research on innovative, long-legged tightly baffled divertor concepts [1–5]. The degree of wall baffling on both the private and common flux sides is kept fixed, as its effect on divertor dissipation will be addressed in a following study. The slot depth is increased by a factor of ≈3 and its effect on the onset and evolution of highly dissipative divertor conditions (i.e. detachment) is evaluated by modeling a range of plasma densities, for both toroidal magnetic field (B_T) directions. Note that this deep slot concept goes beyond the vessel wall, and to make it fit into the vessel, the slot end would need to be aligned to the vessel ceiling, leading to a major loss in plasma core volume and thus detrimental to certain higher power scenarios.

The results presented in this study quantify the benefits of deep slot concepts compared to more shallow geometries, advancing our understanding of the complex interplay between target shaping and particle

* Corresponding author at: Oak Ridge Associated Universities, Oak Ridge, 37830 TN, USA.
E-mail address: maurizior@fusion.gat.com (R. Maurizio).

https://doi.org/10.1016/j.nme.2022.101356
Received 30 June 2022; Received in revised form 20 December 2022; Accepted 23 December 2022
Available online 2 January 2023

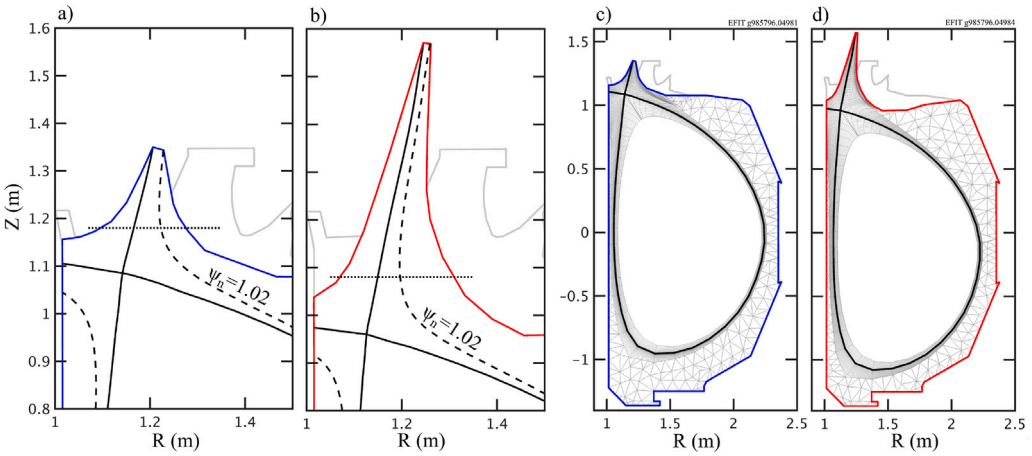

Fig. 1. Shallow slot (a) and deep slot (b) divertor configurations, ending on a flat segment delimited by the magnetic separatrix (black solid line) and the $\psi_n = 1.02$ magnetic surface (black dashed line). The back dotted line represents the slot entrance (throat), the gray contour is the current DIII-D wall geometry. (c–d) Corresponding SOLPS-ITER computational meshes.

drift flows in deep, tightly baffled divertor structures. Moreover, these simulations provide useful physics insights for the design and operation of future fusion devices, e.g. the EXCITE tokamak facility [6] or the SPARC tokamak project [7].

The paper is organized as follows. Section 2 describes the set of inputs to the simulations. The effect of increasing the slot depth is discussed in Section 3 for ion $\mathbf{B}\times\nabla B$ into the divertor, in Section 5 for ion $\mathbf{B}\times\nabla B$ out of the divertor. Section 4 presents the effect of reversing the magnetic field direction. Conclusions are discussed in Section 6.

2. Modeling setup

The modeling described here is performed using the SOLPS-ITER code package [8] (version 3.0.7), which couples the 2D multi-fluid plasma transport code B2.5 [9] and the 3D kinetic neutral transport code EIRENE [10]. B2.5 provides the plasma background to EIRENE, which computes and returns the source and sink terms for plasma particles, momentum and energy due to plasma-neutral collisions. A list of reactions included by EIRENE can be found in [11]. Modeling is carried out for a deuterium plasma with carbon wall and targets. Simulations include neutral–neutral collisions, all particle drifts ($\mathbf{E}\times\mathbf{B}$, $\mathbf{B}\times\nabla B$, viscosity) and the associated currents.

The study considers two divertor configurations, a shallow slot and a deep slot, obtained by altering the DIII-D upper divertor structure, Fig. 1a and 1b. These slot divertors are placed at a smaller major radius than the current upper divertor, where increased triangularity leads to enhanced confinement and stability in the desired scenarios, and have a stronger degree of wall baffling on both the private and common flux sides. The shallow slot is one of the potential candidates for the second phase mission in DIII-D's staged divertor program, while the deep slot considered here would require a significant reduction in core volume in order to fit into the vessel geometry. SOLPS-ITER computational meshes are built using two magnetic equilibria developed with DIII-D's EFIT equilibrium reconstruction code [12], Fig. 1c–d.

Both slot divertors end on a flat surface, extending from the separatrix to the $\psi_n = 1.02$ magnetic surface, or, equivalently, from the $R - R_{\text{sep}} = 0$ to the $R - R_{\text{sep}} \approx 6$ mm surfaces, where $R - R_{\text{sep}}$ is the radial distance from the separatrix at the plasma outboard mid-plane. The width of the slot flat end corresponds to $\approx 4\lambda_q$, where $\lambda_q \approx 1.5$ mm is the Scrape-Off Layer (SOL) power width, estimated by exponential fit of the simulated SOL heat flux profile in proximity of the X-point. In the poloidal plane, the distance between X-point and strike point is 27 and 62 cm for the shallow and deep slot, respectively. The actual slot depth, measured from the slot entrance (black dotted line in Figs. 1a–b) to the strike point, is 18 and 50 cm for the shallow and deep slot, respectively. The increased depth for the latter case results in a ≈5 m longer parallel connection length to the outer target (a 35% increase at ψ_n=1.02).

The cryopump normally located in the private flux region of the upper DIII-D divertor [13] is removed in the current modeling in order to allow for the highest triangularity shapes. The cryopump located below the lower plenum is modeled as a surface absorbing 30% of the impinging particle flux [14]. The plasma grid extends from $R - R_{\text{sep}} = -2$ cm to $R - R_{\text{sep}} = 2$ cm. At the core boundary of the grid, the plasma power flux is set to $P_{\text{SOL}} = 4$ MW, evenly split between electrons and ions [14], to match DIII-D SAS slot divertor modeling [11] and experiments [15]. The average value of the deuterium ion (D^+) density along the core boundary $n_{i,\text{IB}}$ is set to a fixed value, which is changed from case to case to model the evolution of the divertor from attached to detached regime. For $R - R_{\text{sep}} = [-2 : 1]$, particle diffusivity D is set to 0.15 m^2/s and electron thermal diffusivity χ_e is set to 0.5 m^2/s, consistent with prior modeling [14,16,17]. For $R - R_{\text{sep}} = [1 : 2]$ cm, D increases from 0.15 to 1.5 m^2/s and χ_e from 0.5 to 50 m^2/s. This increase of transport in the far-SOL (beyond $\approx 6.5\lambda_q$) is required to have outboard mid-plane plasma density and temperature profiles that resemble, in shape, experimental measurements. Ion thermal diffusivity χ_i is set equal to χ_e. In the divertors, all transport coefficients are increased by a factor of 5. This is necessary to achieve numerical convergence in this set of simulations. Additionally, it accounts for any particle and heat cross-field spreading in the divertor, as discussed in [14]. The plasma flux reaching the vessel wall is recycled as neutrals (D and D_2). At the targets, recycling is set to 100% with standard pre-sheath boundary conditions [18]. At the first-wall surface, recycling is set to 99%. A more detailed description of all SOLPS-ITER boundary conditions can be found in [11].

3. Increase of slot depth for ion $\mathbf{B}\times\nabla B$ into divertor

For ion $\mathbf{B}\times\nabla B$ into the divertor, and for outboard mid-plane separatrix electron density $n_{e,\text{sep}}$ below $\approx 2.5\times10^{19}$ m^{-3}, SOLPS-ITER finds that the electron temperature at the strike point is reduced in the deep slot compared to the shallow slot, Fig. 2b. As a result, the deep slot achieves partial detachment at a lower value of the outboard mid-plane separatrix electron density than the shallow slot. The onset of partial divertor detachment is here defined as when the electron temperature at the strike point drops below 10 eV [19]. Compared to the shallow option, the deep slot achieves $T_{e,\text{OSP}} = 10$ eV with 15% lower upstream separatrix density, Fig. 2b, and $T_{e,\text{OSP}} = 5$ eV with 11% lower upstream separatrix density. The ion saturation current at the strike point also rolls-over approximately when $T_{e,\text{OSP}}$ drops below 10 eV. The target peak parallel heat flux is also reduced in the deep

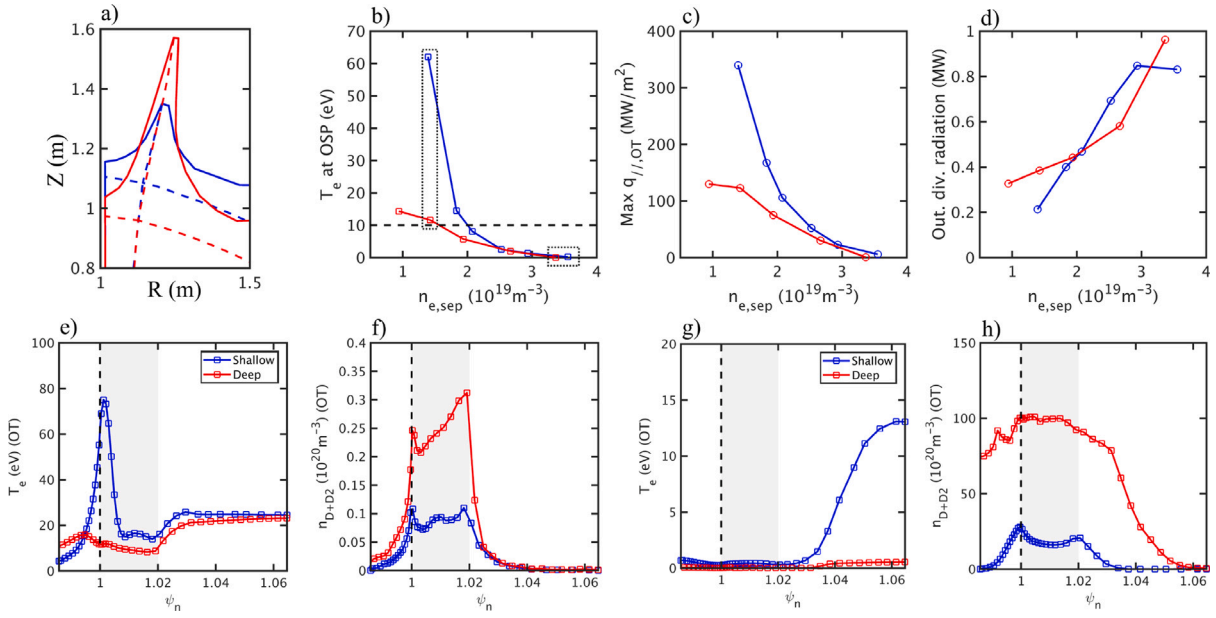

Fig. 2. (a) Shallow (blue) and deep (red) slot geometries, with magnetic separatrix as dashed line. For ion $\mathbf{B}\times\nabla B$ into the divertor, outer strike point electron temperature (b), outer target peak parallel heat flux (c) and outer divertor radiation (d) as a function of outboard mid-plane separatrix electron density, for shallow (blue) and deep (red) slot. (e-f) Outer target profiles of electron temperature and neutral density for fixed $n_{i,\mathrm{IB}} = 2.5\times10^{19}$ m^{-3}, corresponding to $n_{e,\mathrm{sep}} = 1.4\times10^{19}$ m^{-3}. (g–h) Outer target profiles of electron temperature and neutral density for fixed $n_{i,\mathrm{IB}} = 5.5\times10^{19}$ m^{-3}, corresponding to $n_{e,\mathrm{sep}} = 3.5\times10^{19}$ m^{-3}.

slot compared to the shallow slot, Fig. 2c, due to increased divertor radiation, Fig. 2d, in turn due to increased neutral particle density, Fig. 2f. Divertor radiation is dominated by carbon, which radiates ≈ 5 times more than deuterium, and concentrates at the outer target and in the private flux region along the outer divertor leg, from target to x-point. As shown in Fig. 2d, the outer divertor radiation increases with density slower in the deep slot compared to the shallow slot, such that for $n_{e,\mathrm{sep}}$ between ≈ 2 to ≈ 3×10^{19} m^{-3} the radiation is larger in the shallow slot case. SOLPS-ITER finds that, at any density, the plasma in the private flux region close to the x-point and along the outer divertor leg of the deep slot is less dense, warmer and therefore less capable of radiating power compared to the shallow slot. The local particle source is indeed reduced in the deep slot compared to the shallow slot because of the increased distance from the recycling source (the outer target).

For densities above ≈ 2.5×10^{19} m^{-3}, both shallow and deep divertor are partially detached, such that near-SOL quantities like strike point temperature and peak heat flux are similar in both shallow and deep slot. The effect of a deeper slot is, however, clearly visible in the far-SOL. SOLPS-ITER finds that the electron temperature on the slot outboard wall ($\psi_n > 1.02$) is significantly reduced in the deep slot compared to the shallow slot, Fig. 2g, consistent with increased neutral particle density, Fig. 2h. Similarly to low densities, divertor carbon radiation is ≈ 3 times larger than deuterium.

The lower density required for dissipation (and detachment) in the deep slot option can be explained in terms of the slot ability to trap recycled neutrals. SOLPS-ITER finds that the target neutral density increases by a factor of ≈ 3 in the deep slot compared to the shallow slot, Figs. 2f–h, suggesting that the deep slot better confines recycled neutrals, which would explain the increased divertor radiation and, thus, reduced target temperature and heat flux.

The role of slot depth in trapping recycled neutrals is numerically investigated by running the EIRENE kinetic neutral transport code on the plasma solutions produced by SOLPS-ITER. In this run of EIRENE, a large number (10^4) of test particles, neutral D and D_2, are launched from the outer target and their trajectories are followed up to ionization. The typical output of such EIRENE run is shown in Fig. 3a–b, where red and green trajectories represent neutral D and D_2, respectively. From these trajectories, a slot neutral leakage is defined and computed as the fraction of in-slot born particles (above the blue dashed line) that ionize outside of the slot (below the blue dashed line). Analysis of the EIRENE trajectories finds that the slot neutral leakage is reduced in the deep slot compared to the shallow slot at all densities, Fig. 3c. The difference is particularly large at low plasma density, when both slots are attached (strike point temperature above 10 eV). For example, at $n_{e,\mathrm{sep}} = 1.4\times10^{19}$ m^{-3} the neutral leakage is 2.8% for the shallow slot and just 0.1% for the deep slot. This analysis clearly shows that the deeper slot better traps recycling neutrals than the shallow slot, possibly explaining the increased dissipation in the deep slot geometry relative to the shallow slot for the same upstream conditions.

4. Reversal of ion $\mathbf{B}\times\nabla B$ direction

The effect of reversing the B_T direction on the divertor plasma is qualitatively similar in the shallow slot and deep slot. The following section focuses on the shallow slot geometry. SOLPS-ITER finds that the electron temperature at the strike point is reduced with ion $\mathbf{B}\times\nabla B$ out of the slot compared to ion $\mathbf{B}\times\nabla B$ into the slot at all densities, Fig. 4a. The temperature is reduced not only at the strike point, but also along the entire outboard target, as shown in Fig. 4b for outboard mid-plane separatrix electron density of $n_{e,\mathrm{sep}} \approx 1.8\times10^{19}$ m^{-3}. The drastic reduction in temperature is consistent with a pronounced increase in electron density. Specifically, SOLPS-ITER finds that the plasma spreads along the common flux region target for ion $\mathbf{B}\times\nabla B$ out of the divertor, whereas it concentrates on the slot flat end for ion $\mathbf{B}\times\nabla B$ into the divertor, Fig. 4d. These trends are qualitatively consistent with past DIII-D experiments where the outer divertor is either open (un-baffled) [20] or strongly baffled (i.e. the Small-Angle-Slot, SAS, divertor) [15].

The $\mathbf{E}\times\mathbf{B}$ drift flows can explain the divertor solution changes when reversing the ion $\mathbf{B}\times\nabla B$ direction, as explained in previous modeling of DIII-D SAS and SAS-V slot divertors [11,17]. For ion $\mathbf{B}\times\nabla B$ out of the divertor, the $\mathbf{E}\times\mathbf{B}$ drift pushes ions from the private flux region across the separatrix into the common flux region, Fig. 4c, increasing particle recycling on the outer slant, densifying and cooling the SOL plasma, as observed in Fig. 4b–d. For ion $\mathbf{B}\times\nabla B$ into the divertor, instead, the $\mathbf{E}\times\mathbf{B}$ drift has opposite direction, reducing particle recycling on the outer slant, rarefying and warming the SOL plasma.

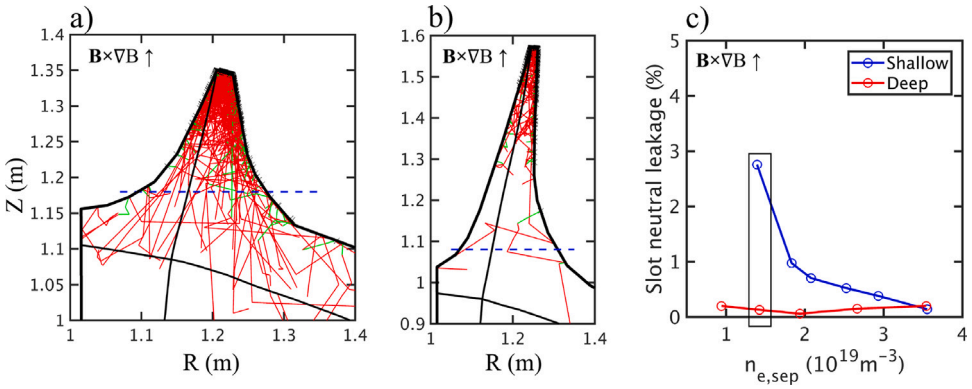

Fig. 3. For ion $\mathbf{B}\times\nabla B$ into the divertor, EIRENE test particle trajectories (red for neutral D, green for D_2) for the shallow (a) and deep (b) slot geometry, at $n_{i,\mathrm{IB}} = 2.5\times10^{19}$ m^{-3}. A total of 10^4 test particles are launched from the outer target and followed until ionization. (c) Slot neutral leakage computed from the EIRENE trajectories, as function of plasma density, for shallow (blue) and deep (red) slot. The highlighted density is shown in subplots (a) and (b).

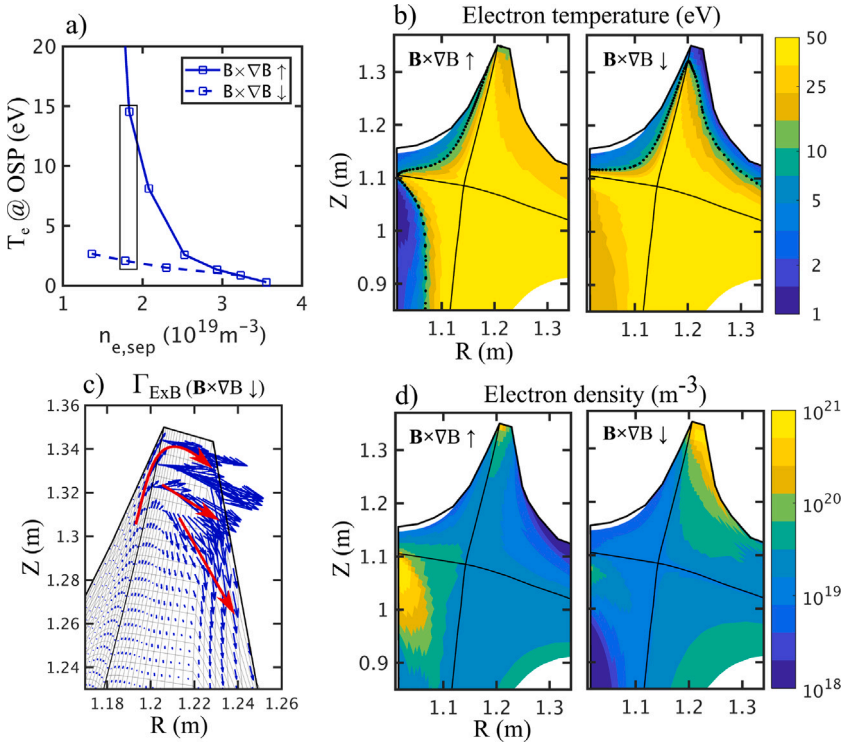

Fig. 4. (a) Outer strike point electron temperature as a function of the outboard mid-plane separatrix electron density, for ion $\mathbf{B}\times\nabla B$ into (solid line) and out of (dashed line) the divertor. At $n_{e,\mathrm{sep}} = 1.8\times10^{19}$ m^{-3}, corresponding to $n_{i,\mathrm{IB}} = 3.0\times10^{19}$ m^{-3} for drift into the divertor and $n_{i,\mathrm{IB}} = 4.0\times10^{19}$ m^{-3} for drift out of the divertor, electron temperature (b) and electron density (d) poloidal maps in the divertor region. The dotted black line in (b) corresponds to the $T_e = 10$ eV contour. (c) At the same density, for ion $\mathbf{B}\times\nabla B$ out of the divertor, ion flux associated to the $\mathbf{E}\times\mathbf{B}$ drift force. Blue arrows are computed by SOLPS-ITER for each mesh cell, red arrows highlight the overall flow direction.

5. Increase of slot depth for ion $\mathbf{B}\times\nabla B$ out of divertor

For ion $\mathbf{B}\times\nabla B$ out of the divertor, SOLPS-ITER finds that the electron temperature at the strike point is reduced in the deep slot compared to the shallow slot at all densities, Fig. 5b, as observed for the opposite B_T direction. The target peak parallel heat flux is also reduced in the deep slot compared to the shallow slot, Fig. 5c, qualitatively consistent with increased divertor radiation, Fig. 5d. At all densities, divertor carbon radiation is ≈ 3 times larger than deuterium. Note that, as in previous modeling of slot divertors [11], SOLPS-ITER finds only detached solutions and fails to converge at lower plasma densities, where attached plasma solutions are expected.

The lower target temperature and heat flux in the deep slot compared to shallow slot can be explained by the better trapping of recycled neutrals, similarly to the opposite B_T direction. EIRENE analysis of 10^4 test particles, launched from the outer target and followed until ionization, finds that the slot neutral leakage fraction is strongly reduced in the deep slot compared to the shallow slot, Fig. 6c. For example, at $n_{e,\mathrm{sep}} = 1.4\times10^{19}$ m^{-3} the neutral leakage is 3.3% for the shallow slot, just 0.7% for the deep slot.

Neutral leakage shows a small dependence on the B_T direction. Neutral leakage factors are larger for ion $\mathbf{B}\times\nabla B$ out of divertor compared to ion $\mathbf{B}\times\nabla B$ in the divertor, compare Fig. 3c to 6c. Additionally, the fraction of particle recycling occurring outside the slot is larger for ion $\mathbf{B}\times\nabla B$ out of divertor than for ion $\mathbf{B}\times\nabla B$ in the divertor, compare Fig. 6a to 3a and 6b to 3b. These differences are an effect of the plasma being closer to the slot exit for ion $\mathbf{B}\times\nabla B$ out of the divertor than for ion $\mathbf{B}\times\nabla B$ into the divertor, Fig. 4b, which shifts the neutral recycling region closer to the slot exit and makes more likely for neutrals to escape the slot.

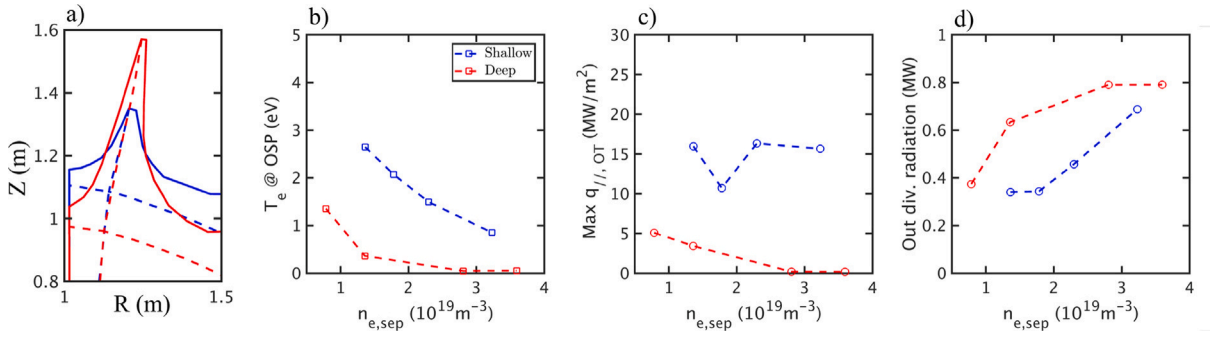

Fig. 5. (a) Shallow (blue) and deep (red) slot geometries, with magnetic separatrix as dashed line. For ion $\mathbf{B}\times\nabla B$ out of the divertor, outer strike point electron temperature (b), outer target peak parallel heat flux (c) and outer divertor radiation (d) as a function of outboard mid-plane separatrix electron density, for shallow (blue) and deep (red) slot.

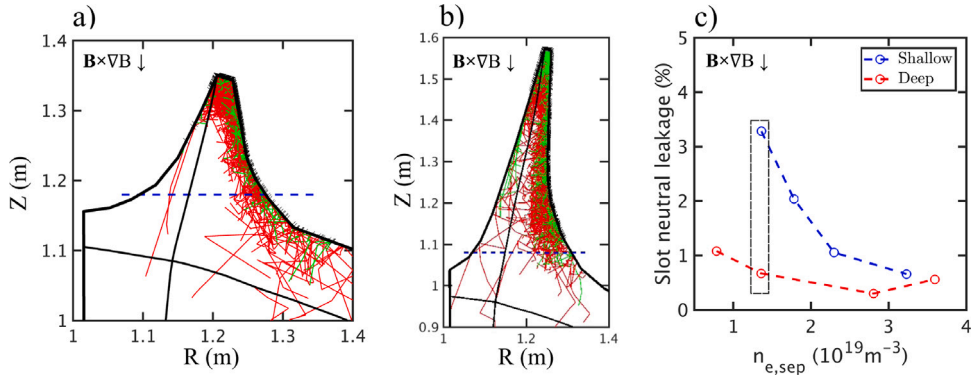

Fig. 6. For ion $\mathbf{B}\times\nabla B$ out of the divertor, EIRENE test particle trajectories (red for neutral D, green for D_2) for the shallow (a) and deep (b) slot geometry, at $n_{i,\mathrm{IB}} = 3.5\times10^{19}$ m^{-3}, corresponding to $n_{e,\mathrm{sep}} = 1.4\times10^{19}$ m^{-3}. A total of 10^4 test particles are launched from the outer target and followed until ionization. (c) Slot neutral leakage computed from the EIRENE trajectories, as function of plasma density, for shallow (blue) and deep (red) slot. The highlighted density is shown in subplots (a) and (b).

6. Conclusions

A staged divertor program is currently under discussion to advance DIII-D research on core-edge integration. One phase could address optimization of power and particle exhaust in DIII-D upper divertor. Supporting modeling of several slot divertor options is underway, including variations in wall baffling, slot depth and divertor leg length. This paper specifically focuses on the role of slot depth to achieve highly dissipative (detached) divertor conditions, using the SOLPS-ITER code package including the effect of particle drifts.

For ion $\mathbf{B}\times\nabla B$ into the divertor, the direction typically associated with lower power threshold for H-mode access, SOLPS-ITER finds that increasing the slot depth from 18 to 50 cm reduces the target electron temperature and peak heat flux, due to increased divertor radiation. As a result, the transition to $T_e < 10$ eV at the outer strike point occurs at a 15% lower value of upstream density. A detailed characterization of neutral trapping dependence on slot geometry is achieved by running the EIRENE kinetic neutral transport code, where 10^4 neutral test particles are launched from the outer target and followed up to ionization. Analysis of the neutrals' trajectories reveals that leakage from the slot is significantly reduced in the deep slot compared to the shallow slot, at all densities, thus explaining the increased divertor radiation and lower detachment density threshold. Reversing the B_T direction significantly impacts the divertor plasma solution, which can be explained as an effect of the $\mathbf{E}\times\mathbf{B}$ particle flow. As for the opposite B_T direction, the deep slot has lower temperature and reduced neutral leakage compared to the shallow slot.

This work shows that increasing the depth of a slot divertor, at fixed degree of wall baffling, is beneficial to achieve highly dissipative (detached) divertor conditions for both field directions, because it reduces leakage of recycled neutral particles. Additional modeling could build on these results to assess the effect of slot depth on leakage of low-Z impurities. This would provide essential physics insights to support detachment experiments where divertor cooling is achieved by puffing low-Z impurities in the divertor.

CRediT authorship contribution statement

R. Maurizio: Conceptualization, Data curation, Formal analysis, Investigation, Methodology, Project administration, Software, Visualization, Writing. **A.W. Leonard:** Supervision, Validation. **A.G. McLean:** Supervision, Validation. **M.W. Shafer:** Supervision, Writing – review & editing. **P.C. Stangeby:** Supervision, Writing – review & editing. **D. Thomas:** Supervision, Funding acquisition. **J.H. Yu:** Supervision, Validation.

Declaration of competing interest

The authors declare that they have no known competing financial interests or personal relationships that could have appeared to influence the work reported in this paper.

Data availability

Data will be made available on request.

Acknowledgments

The authors would like to thank the entire DIII-D Divertor Science and Innovation team for their help and constructive discussions. This material is based upon work supported by the U.S. Department of Energy, Office of Science, Office of Fusion Energy Sciences, using the DIII-D National Fusion Facility, a DOE Office of Science user facility, under Award(s) DE-FC02-04ER54698 and DE-AC05-00OR22725.

Disclaimer

References

[1] G. Fishpool, et al., MAST-upgrade divertor facility and assessing performance of long-legged divertors, J. Nucl. Mater. 438 (2013) S356–S359, http://dx.doi.org/10.1016/j.jnucmat.2013.01.067.

[2] M. Wigram, et al., Performance assessment of long-legged tightly-baffled divertor geometries in the ARC reactor concept, Nucl. Fusion 59 (2019) http://dx.doi.org/10.1088/1741-4326/ab394f.

[3] M. Umansky, et al., Study of passively stable, fully detached divertor plasma regimes attained in innovative long-legged divertor configurations, Nucl. Fusion 60 (2020) http://dx.doi.org/10.1088/1741-4326/ab46f4.

[4] C. Sang, et al., SOLPS analysis of neutral baffling for the design of a new diverter in DIII-D, Nucl. Fusion 57 (2017) http://dx.doi.org/10.1088/1741-4326/aa6548.

[5] I. Senichenkov, et al., SOLPS-ITER modeling of CFETR advanced divertor with ar and ne seeding, Nucl. Fusion 62 (2022) http://dx.doi.org/10.1088/1741-4326/ac75da.

[6] T. Carter, et al., Powering the future: Fusion and plasmas, Report (FESAC, 2020), 2020, available at https://usfusionandplasmas.org/wp-content/themes/FESAC/FESAC_Report_2020_Powering_the_Future.pdf.

[7] P. Rodriguez-Fernandez, et al., Overview of the SPARC physics basis towards the exploration of burning-plasma regimes in highfield, compact tokamaks, Nucl. Fusion 62 (2022) http://dx.doi.org/10.1088/1741-4326/ac1654.

[8] X. Bonnin, et al., Presentation of the new SOLPS-ITER code package for tokamak plasma edge modelling, Plasma and Fusion Res. 11 (2016) http://dx.doi.org/10.1585/pfr.11.1403102.

[9] R. Schneider, et al., Plasma edge physics with B2-eirene, Contrib. Plasma Phys. 46 (2006) 3–191, http://dx.doi.org/10.1002/ctpp.200610001.

[10] D. Reiter, et al., The EIRENE and B2-EIRENE codes, Fusion Sci. Technol. 47 (2005) 172–186, http://dx.doi.org/10.13182/FST47-172.

[11] R. Maurizio, et al., Numerical assessment of the new v-shape small-angle slot divertor on DIII-D, Nucl. Fusion 61 (2021) 116042, http://dx.doi.org/10.1088/1741-4326/ac27c8.

[12] L. Lao, et al., Reconstruction of current profile parameters and plasma shapes in tokamaks, Nucl. Fusion 25 (1985) http://dx.doi.org/10.1088/0029-5515/25/11/007.

[13] A.S. Bozek, et al., Pumping characteristics of the DIII-D cryopumps, in: 18th IEEE/NPSS Symposium on Fusion Engineering. Symposium Proceedings (Cat. No. 99CH37050), 1999, pp. 523–526, http://dx.doi.org/10.1109/FUSION.1999.849893.

[14] E. Meier, et al., Modeling $E\times B$ drift transport in conceptual slot divertor configurations, Contrib. Plasma Phys. 60 (2020) e201900151, http://dx.doi.org/10.1002/ctpp.201900151.

[15] H.Y. Guo, et al., First experimental tests of a new small angle slot divertor on DIII-D, Nucl. Fusion 59 (2019) http://dx.doi.org/10.1088/1741-4326/ab26ee.

[16] T.D. Rognlien, et al., Comparison of 2d simulations of detached divertor plasmas with divertor thomson measurements in the DIII-D tokamak, Nucl. Mater. Energy 12 (2017) 44–50, http://dx.doi.org/10.1016/j.nme.2016.12.002.

[17] X. Ma, et al., First evidence of dominant influence of $E\times B$ drifts on plasma cooling in an advanced slot divertor for tokamak power exhaust, Nucl. Fusion 61 (2021) 054002, http://dx.doi.org/10.1088/1741-4326/abde75.

[18] H. Du, et al., Manipulation of ExB drifts in a slot divertor with advanced shaping to optimize detachment, Nucl. Fusion 60 (2020) http://dx.doi.org/10.1088/1741-4326/abb53f.

[19] P.C. Stangeby, et al., Basic physical processes and reduced models for plasma detachment, Plasma Phys. Control. Fusion 60 (2018) http://dx.doi.org/10.1088/1361-6587/aaacf6.

[20] A. Jaervinen, et al., Impact of drifts on divertor power exhaust in DIII-D, Nucl. Materials and Energy 19 (2019) 230–238, http://dx.doi.org/10.1016/j.nme.2019.02.023.